symmetry

MDPI

Article

The Effect of Nanoparticle Shape and Microchannel Geometry on Fluid Flow and Heat Transfer in a Porous Microchannel

Zahra Abdelmalek [1,2], Annunziata D'Orazio [3] and Arash Karimipour [4,*]

[1] Institute of Research and Development, Duy Tan University, Da Nang 550000, Vietnam; zahraabdelmalek@duytan.edu.vn
[2] Faculty of Medicine, Duy Tan University, Da Nang 550000, Vietnam
[3] Dipartimento di Ingegneria Astronautica, Elettrica ed Energetica, Sapienza Università di Roma, Via Eudossiana 18, 00184 Roma, Italy; annunziata.dorazio@uniroma1.it
[4] Sustainable Management of Natural Resources and Environment Research Group, Faculty of Environment and Labour Safety, Ton Duc Thang University, Ho Chi Minh City, Vietnam
* Correspondence: arashkarimipour@tdtu.edu.vn

Received: 4 March 2020; Accepted: 2 April 2020; Published: 8 April 2020

Abstract: Microchannels are widely used in electrical and medical industries to improve the heat transfer of the cooling devices. In this paper, the fluid flow and heat transfer of water–Al_2O_3 nanofluids (NF) were numerically investigated considering the nanoparticle shape and different cross-sections of a porous microchannel. Spherical, cubic, and cylindrical shapes of the nanoparticle as well as circular, square, and triangular cross-sections of the microchannel were considered in the simulation. The finite volume method and the SIMPLE algorithm have been employed to solve the conservation equations numerically, and the k-ε turbulence model has been used to simulate the turbulence fluid flow. The models were simulated at Reynolds number ranging from 3000 to 9000, the nanoparticle volume fraction ranging from 1 to 3, and a porosity coefficient of 0.7. The results indicate that the average Nusselt number (Nu_{ave}) increases and the friction coefficient decreases with an increment in the Re for all cases. In addition, the rate of heat transfer in microchannels with triangular and circular cross-sections is reduced with growing Re values and concentration. The spherical nanoparticle leads to maximum heat transfer in the circular and triangular cross-sections. The heat transfer growth for these two cases are about 102.5% and 162.7%, respectively, which were obtained at a Reynolds number and concentration of 9000 and 3%, respectively. However, in the square cross-section, the maximum heat transfer increment was obtained using cylindrical nanoparticles, and it is equal to 80.2%.

Keywords: nanoparticle shape effect; porous medium; turbulent flow; different cross-sections

1. Introduction

It is possible to improve the heat transfer rate of the fluids by flow geometry or boundary conditions improvement as well as improve the thermophysical properties of the fluid such as the thermal conductivity coefficient. One of the most desirable ways of thermal conductivity coefficient enhancement of the base fluid is adding fine solid particles to the base fluid [1–9]. It could also be improved using a porous medium in the channel [10–15].

Previous studies are reviewed below. In the review, articles about porous media are first discussed. Subsequently, articles on microchannels will be reviewed and finally, the limitations of the porous media in microchannels will be discussed.

Jiang et al. [16] conducted an experimental and numerical study of heat transfer in a microchannel filled with porous materials. Their results show that the heat transfer and pressure drop in a microchannel filled with porous materials are larger than those in a simple microchannel. Hatami and D. D. Ganji [17] numerically investigated the heat transfer and water–copper nanofluid (NF) flow in a microchannel heat sink using the porous media approach. They studied the effects of the nanoparticle concentration, porosity coefficient, Darcy number, and microchannel dimensions on the hydrothermal behavior of the NF flow. Their results revealed that the heat transfer will increased by the volume fraction enhancement, resulting in less temperature difference between the coolant and wall temperature.

Ghazvini and Shokouhmand [18] numerically investigated the influence of NF on the cooling of a heat sink microchannel using fins and a porous medium. They showed that the dimensionless temperature and Nu_{ave} can be enhanced by a porosity coefficient increment. Goodarzi et al. [19] numerically studied the effect of slip velocity and temperature jump on the NF flow in the microchannel filled with porous materials. Their results show that in higher Reynolds numbers, the local Nusselt number (Nu) enhanced significantly. Moreover, a lower permeability leads to a higher local Nu.

Ting et al. [20] numerically studied the effect of entropy generation on the NF flow and heat transfer in a microchannel filled with a non-equilibrium porous medium. Their results indicate that adding the porous medium improves heat transfer and entropy generation. Arabpoor et al. [21] performed a numerical study on the influence of the slip boundary condition on NF flow in a microchannel. According to their results, the Nu_{ave} increases by a higher nanoparticle volume fraction and Re enhancement.

In summing up the studies on porous media [16–21], it can be concluded that the application of porous media, in all geometries studied, has significantly increased the rate of heat transfer and pressure drop. It is important to note which of these factors are most important in each application. It makes clear whether the use of porous media is justified or not.

Hosseini and Sheikholeslami [22] numerically examined the impact of a magnetic field and entropy generation on the flow field and heat transfer inside a two-dimensional microchannel. Their results show that the total entropy generation is higher for a larger porosity coefficient.

Ali Akbari et al. [23] conducted a numerical study on the influence of the ribs height on the heat transfer and water–aluminum oxide NF flow in a microchannel. Their results demonstrated that the tooth height and the concentration have a direct influence on the friction coefficient and Nu_{ave}.

Karimipour et al. [24] numerically studied the effect of vortex generators on the fluid flow and heat transfer in a two-dimensional microchannel. Their results show that the heat transfer significantly increases by a higher Re and volume fraction as well as more vortex generators. Reza et al. [25] numerically investigated the effect of triangular teeth on heat transfer and non-Newtonian NF flow in a microchannel with a rectangular cross-section. According to their results, heat transfer was influenced directly by the nanoparticle volume fraction, and the smaller diameter of the nanoparticles leads to the higher heat transfer of the microchannel. Arabpour et al. [26] have conducted a numerical study of the slip boundary condition on the heat transfer and Multi-walled carbon nanotubes (MWCNT)–water in a microchannel. Their results showed that the temperature remarkably decreases with an increment in the slip velocity coefficient on the solid surfaces, whilst it improves the heat transfer.

Avramenko et al. [27] numerically investigated the impact of mixed convection in a vertical microchannel with a circular cross-section. They found that the shape of the cross-section has a significant effect on the Nu_{ave}. Gao and Jian [28] proposed an analytical solution of magnetohydrodynamic fluid flow in a microchannel with a circular cross-section. According to their results, the volumetric flow rate grew and then decreased with the Hartmann number. El Mghari [29] conducted an experimental and numerical investigation on the effect of condensation on the thermal performance of a microchannel with a square cross-section. Their results indicate that the average and local Nu are strongly dependent on the heat flux through the wall.

Kiyasatfar and N. Pourmahmoud [30] numerically examined the heat transfer of a non-Newtonian NF in a square microchannel. Their results show that the Nu_{ave} rises happened by Re and nanoparticle

volumetric percentage growth. Ferrari et al. [31] conducted a numerical study on the effect of boiling inside a two-dimensional microchannel with a square cross-section. They found that for all Res, the bubble velocity in the channel with the square cross-section is higher than the other ones. Bahmanpour et al. [32] numerically studied the influence of various teeth on the heat transfer and NF flow in a microchannel. Their results show that an increment in the velocity of the NF leads to a significant improvement of the Nu_{ave} and the thermal hydraulic performance. Weng et al. [33] carried out an experimental and numerical study on the effect of ribs on heat transfer in the microchannel. According to their findings, the presence of vortex generators will improve the thermal performance of the microchannel.

From the studies reviewed on microchannels [22–33], it can be concluded that the use of microchannels, due to the increasing need of different industries for small and efficient heat exchangers, is considered to be more than before. Therefore, the behavior of microchannels in different environments needs to be given more attention.

Dejam [34] numerically investigated the effect of the electro-osmotic scattering coefficient on a viscoelastic microchannel flow filled with porous materials. He concluded that the ratio of the dispersion coefficient in a microchannel with a porous wall to a nonporous-walled microchannel is significantly reduced by the degree of fluid velocity. In addition, the ratio of the microchannel scattering coefficient to the nonporous-walled microchannel reduces the degree of fluid elongation.

In another paper, he [35] also numerically investigated the effect of hydrodynamic scattering inside a microchannel filled with porous materials. Their results show that the Peclet number and bluntness parameter improve the behavior of the hydrodynamic scattering coefficient in the porous microchannel. They also concluded that the mass transfer in a porous-walled microfluidic channel is also slower than mass transfer in a nonporous-walled microfluidic channel.

Past studies [34,35] indicate that few studies have been conducted on the existence of porous media in microchannels. Olayiwola and Dejam [36] experimentally studied the viscosity behavior of silica NFs with different electrolyte ions. Their results indicate that changes in oil recovery when injecting nanoparticles into the tank may alter the viscosity behavior of the liquid in the porous medium in addition to changing the angle of contact and damage. In another research, they [37] evaluated the effect of surface energy on dissolving nanoparticles, surfactants, and electrolytes. Their results show that the dipole–dipole interaction of ions contributes to the reduction of interfacial energy by adding the EDL effect. There have also been recent studies in the field that address similar issues [38–52].

Based on previous studies, it can be concluded that the effect of using nanofluid in a microchannel filled with porous media has not been investigated simultaneously. Moreover, the effect of the nanoparticles' shape and geometrical cross-section on the thermal behavior of such microchannels has not been considered. The aim of this study is to examine the influence of the shape of aluminum oxide nanoparticles on the flow field and heat transfer inside microchannels with various cross-sections. Therefore, spherical, cubic, and cylindrical nanoparticles have been studied in microchannels with circular, square, and triangular cross-sections. The study involves a Re range of 3000 to 9000, nanoparticle volume percentages ranging from 1 to 3, and a porosity coefficient of 0.7. The aim and innovation of this work is to select the best shape of the nanoparticles and the best cross-section in the microchannel in terms of thermal hydraulic criteria.

2. Problem Statement and Numerical Simulation

2.1. Problem Definition

Figure 1 displays the computational space along with its boundary conditions. The inside of the computational space is considered to be porous during the problem solution.

According to reviews on similar articles, the Reynolds number range was in the range of ($3000 \leq Re \leq 9000$). Moreover, in microchannels, usually the velocity values are no higher than the speeds associated with these Reynolds numbers.

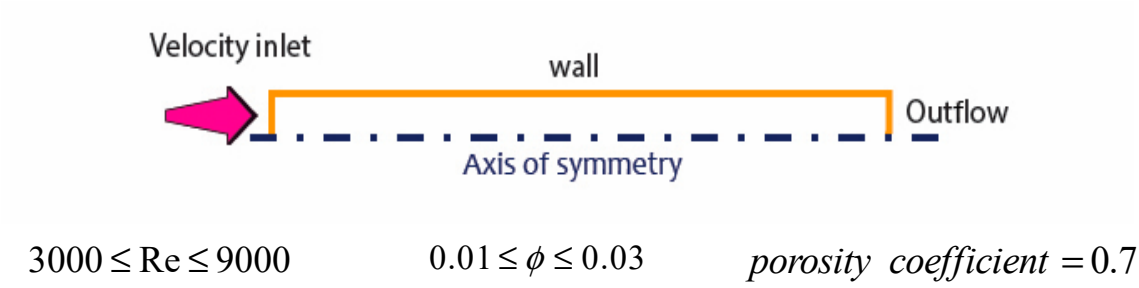

Figure 1. Schematic of the microchannel and general sketch of the problem.

The flow and heat transfer of the NF in the microchannel are investigated for the case where the microchannel is filled with porous material. The computational space in the present paper is defined as follows. The effects of different shapes of aluminum oxide nanoparticles are investigated so as to achieve more practical results. The cross-sections used for the microchannel are shown in Figure 2a. The radius of the circular cross-section and the side lengths of the square and triangular cross-sections are selected such that the resulted cross-sectional areas are identical. The hydraulic radius of each cross-section is displayed in Figure 2a. The NF is defined as single-phase, and effective physical properties are used in the equations. Different shapes are considered for the nanoparticle, as shown in Figure 2b.

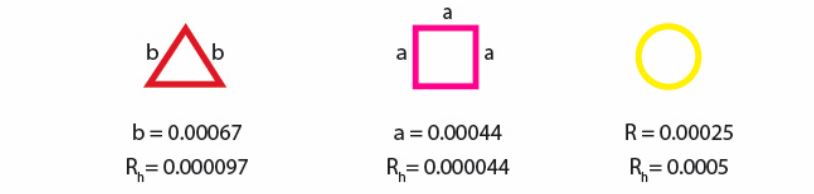

(**a**) The hydraulic radius for the different cross-sections

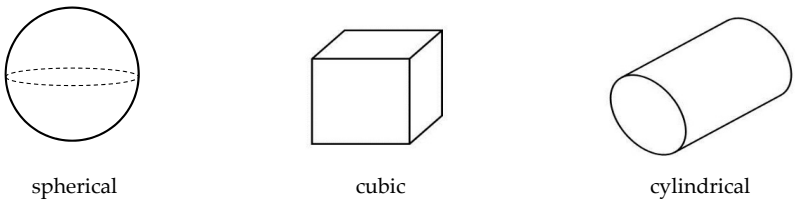

(**b**) 3D representation of the nanoparticles

Figure 2. Hydraulic radius and 3D geometry of the nanoparticles.

2.2. Formulation

According to the various sources, different relationships that define fluid properties can be employed for different nanoparticle shapes. The effective properties used for the three considered nanoparticles are as follows [53]:

Spherical:

$$\rho_{eff} = (1-\phi)\rho_f + \phi\rho_s \tag{1}$$

$$c_{p_{eff}} = \frac{(1-\phi)(\rho c_p)_f + \phi(\rho c_p)_s}{\rho_{eff}} \tag{2}$$

$$\frac{k_{eff}}{k_s} = \frac{k_p + 2k_s + 2\phi(k_p - k_s)}{k_p + 2k_s - \phi(k_p - k_s)} \tag{3}$$

$$\mu_{eff} = \mu_s(1 + 2.5\phi + 6.2\phi^2) \tag{4}$$

Cylindrical:

$$\rho_{eff} = (1-\phi)\rho_f + \phi\rho_s \tag{5}$$

$$c_{p_{eff}} = \frac{(1-\phi)(\rho c_p)_f + \phi(\rho c_p)_s}{\rho_{eff}} \tag{6}$$

$$\frac{k_{eff}}{k_s} = 1 + 3.95\phi \tag{7}$$

$$\mu_{eff} = \mu_s(1 + 13.5\phi + 904.4\phi^2) \tag{8}$$

Cubic:

$$\rho_{eff} = (1-\phi)\rho_f + \phi\rho_s \tag{9}$$

$$c_{p_{eff}} = \frac{(1-\phi)(\rho c_p)_f + \phi(\rho c_p)_s}{\rho_{eff}} \tag{10}$$

$$\frac{k_{eff}}{k_s} = 1 + 3.37\phi \tag{11}$$

$$\mu_{eff} = \mu_s(1 + 1.9\phi + 471.4\phi^2) \tag{12}$$

The above relationships are substituted into the simulation equations, and the obtained fluid properties were replaced. The porosity considered to be 0.7 in this research.

The porous solid matrix is considered to be isotropic and homogeneous. In the steady state and a fully developed flow, $V = 0$ and $u = u(y)$. The Darcy–Brinkman momentum equation has been used.

3. Meshing

Structured meshes have been utilized whenever possible for meshing the computational space in this study. In numerical works, one tries to use structured meshes as much as possible, and this model can be employed for the geometries with circular and square cross-sections.

Figure 3a shows the mesh generation for the square cross-section. A rectangular mesh has been used here. As seen in Figure 3b, an unstructured grid is used in case of the triangular cross-section in order to be able to completely cover the overall computational domain.

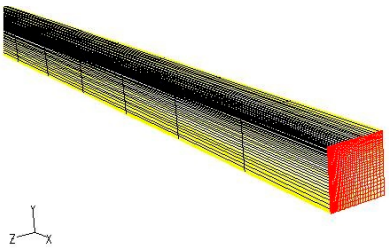

(**a**) Generated mesh for square cross-section

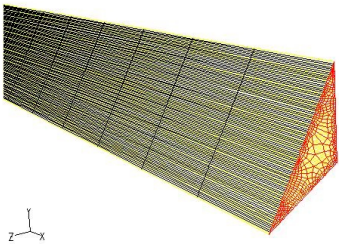

(**b**). Generated mesh for triangular cross-section

Figure 3. Microchannel meshing.

3.1. Boundary Conditions

Some boundary conditions were applied to solve the problem. The microchannel walls are assumed to be under a constant heat flux. Table 1 lists the inlet conditions used in this paper to obtain the initial results for validation. As shown in this table, the inlet fluid velocity increases by Re.

Table 1. Inlet conditions for various Re.

Inlet Velocity	Reynolds
6.03	3000
10.05	5000
14.07	7000
18.09	9000

The modeling conditions are represented in Table 2. A 2D model simulation was considered for the circular cross-section, whereas the problem modeled square and triangular cross-sections three dimensionally. Moreover, the steady-state condition was considered over the solution, and a turbulence model was used for fluid flow modeling. A model with two equations is utilized to simulate the flow disturbance, and the fluid behavior near the wall is modeled using the standard function.

Table 2. Modeling conditions.

Two-Dimensional (Flow Modeling with Circular Cross-Section) Three-Dimensional (Flow Modeling with Square and Triangular Cross-Sections)	**Computational Domain**
Steady-state	Time-dependence
Nonlinear $k-\varepsilon$	Turbulence model
Use of standard wall function	Behavior near the wall
Active	Equation of conservation of energy

The equations used for the numerical solution are shown in Table 3. As seen in this table, six equations are required to model the fluid motion and heat transfer in a porous medium.

Table 3. Required equations and their number used for modeling.

Quantity	Equations
1	Continuity
2 (for flow in the circular cross-section) 3 (for flow in the triangular and square cross-sections)	Navier–Stokes
1	Energy
2	Turbulence

A continuity equation expressing that no fluid mass is created nor destroyed, two momentum equations—One along the flow and another perpendicular to it—Are required (three momentum equations are utilized for square and triangular cross-sections). It should be noted that the terms related to the flow in the porous medium have also been added to the equations. In Table 4, under relaxation coefficients are presented.

The energy equation is also used in the problem solving. It must be noted that energy can be analyzed in two ways. One way is to consider one equation for energy balance between the porous state and the fluid. The other way is to use two independent equations, where one is used for modeling heat transfer in the porous medium and the other corresponds to the fluid flowing through it.

The discretization of the equations is presented in Table 5. The SIMPLE algorithm is used for the solution in this problem, and all the equations have been discretized using the upwind scheme. In order to obtain a better approximation, second-order discretization is used, and all the equations are discretized on the computational points in order to turn into algebraic equations. At this stage, a

function must be defined to specify the relationship between pressure and velocity. This function is known as the SIMPLE algorithm.

Table 4. Under-relaxation coefficients.

Value	Equations
0.3	Pressure
0.7	Momentum
0.8	Turbulence energy
0.8	Turbulence energy dissipation rate
1	Energy

Table 5. Discretization method.

Method	Term in Equations
Standard	Pressure
Upwind	Momentum
Upwind	Turbulence energy
Upwind	Turbulence energy dissipation rate
Upwind	Energy

Finally, it must be noted that the fluid used in this study is a NF and it has been modeled as single phase. The base fluid and aluminum oxide properties are listed in Table 6.

Table 6. Physical properties of water and nanoparticles [54].

Water	Aluminum Oxide	Physical Properties
997.1	3970	$\rho(kg/m^3)$
0.00089	-	$\mu(Pa.s)$
4179	765	$c_P(J/kg.K)$
0.6	40	$k(W/m.K)$

3.2. Grid Independence

First, the considered geometry was modeled and meshed in Design Modeler software. This geometry was used for several different grids, and the Nu was calculated at the Re of 9000 (Tables 7–9). As can be seen from this table, the Nu suddenly changes at some point, after which the Nu can be assumed to be almost constant, and the so-called grid-independence is achieved. Given the cross-sectional geometry, different meshes are used, and the criterion for choosing the right point is the lack of change in the results with an increment in the number of nodes (i.e., finer mesh) after that point.

Table 7. Grid independence for the circular pipe.

Number of Cells	Nusselt Number
35×250	0.85515696
40×250	0.8424636
45×250	55.56332
50×250	52.42397
55×250	51.91109

Table 8. Grid independence for the square pipe.

Number of Cells	Nusselt Number
$35 \times 35 \times 250$	1.567
$40 \times 40 \times 250$	15.67
$45 \times 45 \times 250$	32.11
$50 \times 50 \times 250$	34.987
$55 \times 55 \times 250$	35.678

Table 9. Grid independence for the triangular pipe.

Number of Cells	Nusselt Number
35 × 35 × 250	8.674
40 × 40 × 250	23.12
45 × 45 × 250	65.14
50 × 50 × 250	73.98
55 × 55 × 250	74.134

3.3. Validation

In order to validate the numerical results, the geometry of the microchannel in the work by Arjun and Rakesh [55] has been simulated, and the results relating to the Nu_{ave} have been compared to the results of their work, as shown in Figure 4. It can be seen that there is merely an inconsiderable difference between the Nu_{ave} obtained in this paper and that of Arjun and Rakesh [55]. The error is just about 4.832%, which confirms the results' validity.

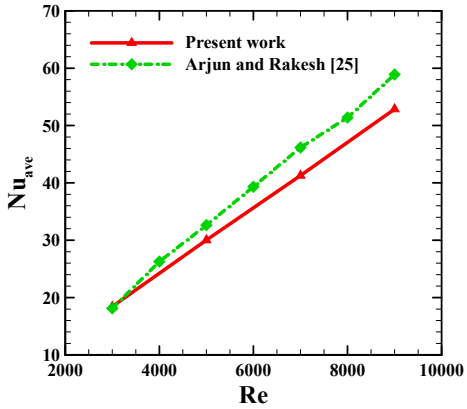

Figure 4. Validation of the present study with Arjun and Rakesh [55] results.

4. Results and Discussion

Three different nanoparticle geometries were used for the circular cross-section. Four different Re values of 3000, 5000, 7000, and 9000, and three volume fractions of 0.01, 0.02, and 0.03 are examined. The results of the effects of these parameters on the thermohydraulic characteristics of the nanofluid flow are presented in the following sections.

4.1. Nusselt Number in the Microchannel with the Circular Cross-Section

As can be seen from Figure 5, for the spherical nanoparticle, the Nu increases with growing Re and decreases with growing NF concentration. The Re enhancement accelerates the fluid near the wall, resulting in heat transfer enhancement, and so the Nu will increased. In many problems, the Nu increases by increasing the NF concentration due to the higher thermal conductivity coefficient and heat transfer. However, in this problem, the Nu and heat transfer rate decrease with an increment in the NF concentration, similar to numerous other problems studied so far [10–12,18,20]. The Nu reduction over the NF concentration accretion is more considerable for higher Re values.

It can be observed in Figure 5b that the Nu for the cylindrical nanoparticle is smaller than of the spherical and cubic nanoparticles, at a concentration of 0.02. Moreover, the Nusselt number for the spherical nanoparticle is larger than that for the cubic nanoparticles, and this difference increases for larger Re values. As shown in Figure 5c, the Nu_{ave} for the cylindrical nanoparticle is smaller than that for the spherical and cubic nanoparticles at a concentration of 0.03. It is also can be concluded that the Nu_{ave} for the spherical nanoparticle is larger than the cubic nanoparticles, and this difference increases for larger Re values. This observation was the same for a concentration of 0.02.

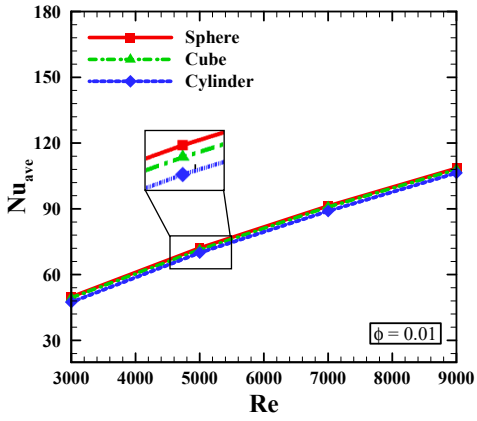

(**a**) Average Nusselt number in ϕ=0.01

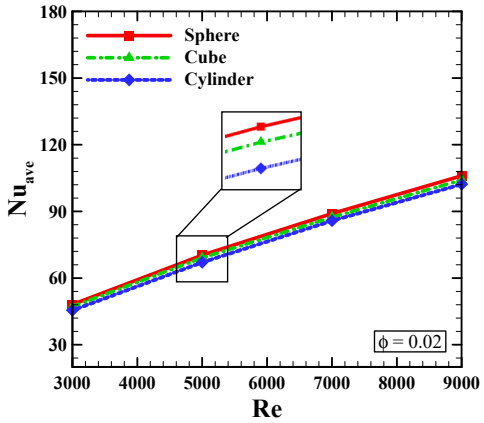

(**b**) Average Nusselt number in ϕ=0.02

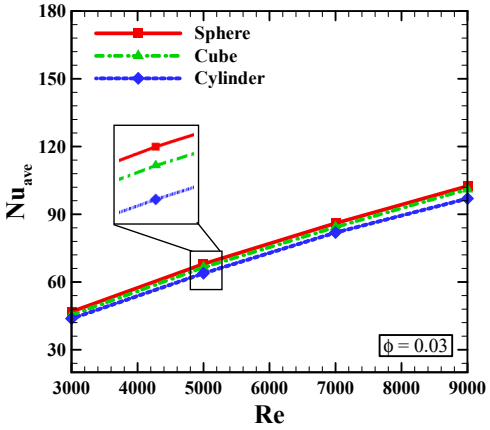

(**c**) Average Nusselt number in ϕ=0.03

Figure 5. Nu_{ave} vs. Re for a porosity coefficient of 0.7 and for different volume fractions in a microchannel with a circular cross-section.

4.2. Friction Coefficient for the Microchannel with the Circular Cross-Section

Figure 6 plotted the friction coefficient versus Re. As shown in this figure, the friction coefficient is a decreasing function of Re. It is also can be observed that the friction coefficient increases by NF concentration enhancement, and the variation of this coefficient with NF concentration is more significant at lower Re values.

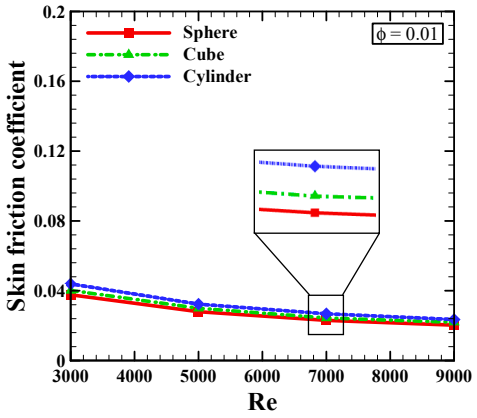

(**a**) Friction coefficient in ϕ=0.01

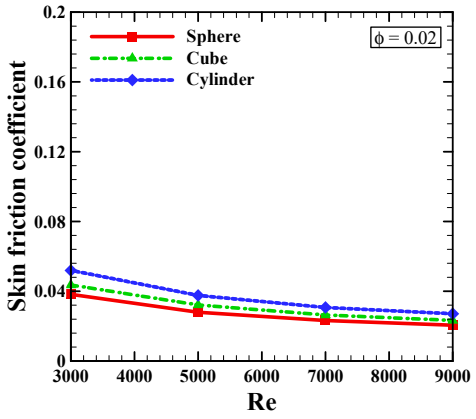

(**b**) Friction coefficient in ϕ=0.02

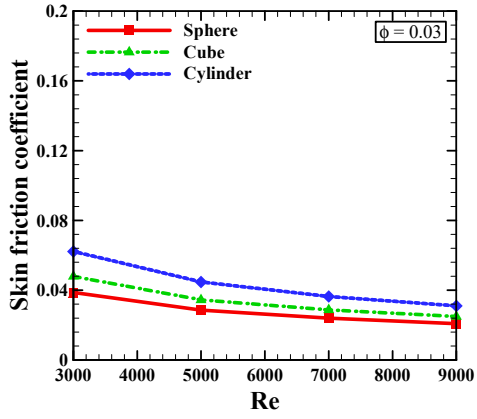

(**c**) Friction coefficient in ϕ=0.03

Figure 6. Friction coefficient vs. Re for a porosity coefficient of 0.7 and for different volume fractions in a microchannel with a circular cross-section.

4.3. Average Nusselt Number in the Microchannel with the Square Cross-Section

Figure 7 show the Nu versus Re for various NF concentrations in a square microchannel with a spherical nanoparticle. As can be seen from this figure, the Nusselt number increases by Re and NF concentration enhancement. It is also observed that the Nu decreases using a square cross-section instead of a circular one. Moreover, the Nu for cubic and cylindrical nanoparticles has trends identical to that of the spherical nanoparticle. In other words, the Nu is a growing function of the Re and the nanoparticle concentration.

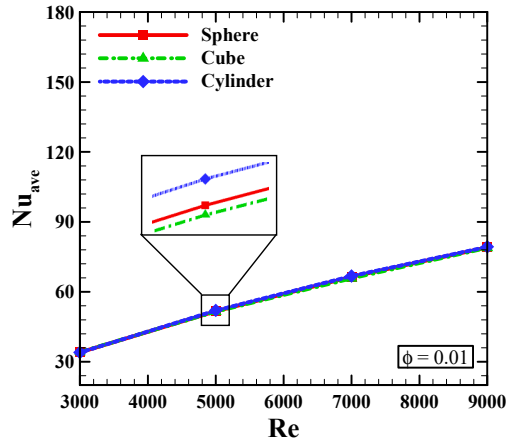

(**a**) Average Nusselt number in ϕ=0.01

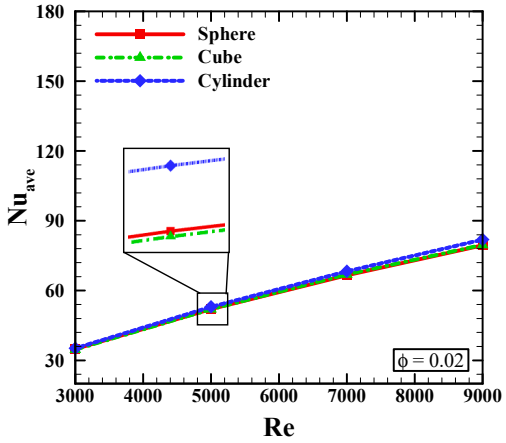

(**b**) Average Nusselt number in ϕ=0.02

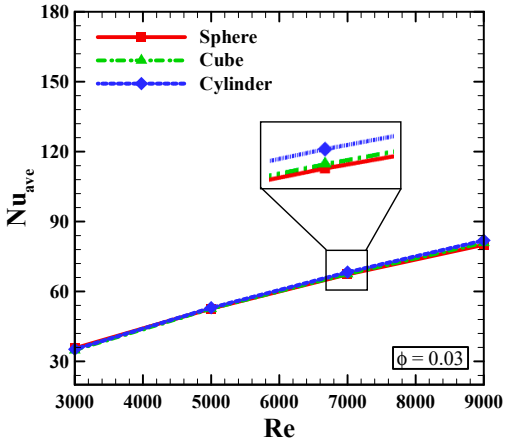

(**c**) Average Nusselt number in ϕ=0.03

Figure 7. Nu_{ave} vs. Re for a porosity coefficient of 0.7 and for different volume fractions in a microchannel with a square cross-section.

4.4. Friction Coefficient for the Microchannel with the Square Cross-Section

The plots of friction coefficient and heat transfer, as shown in Figure 8, exhibit identical behaviors for spherical, cylindrical, and cubic nanoparticles. As can be seen from this figure, the friction coefficient is an increasing function of Re and NF concentration for all cases, and slope of the plot is steeper when cubic and cylindrical nanoparticles are used.

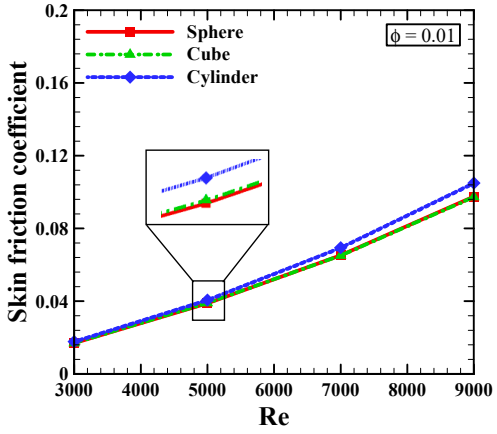

(**a**) Friction coefficient in ϕ=0.01

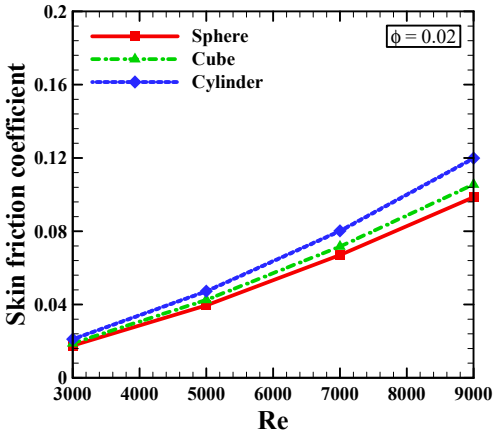

(**b**) Friction coefficient in ϕ=0.02

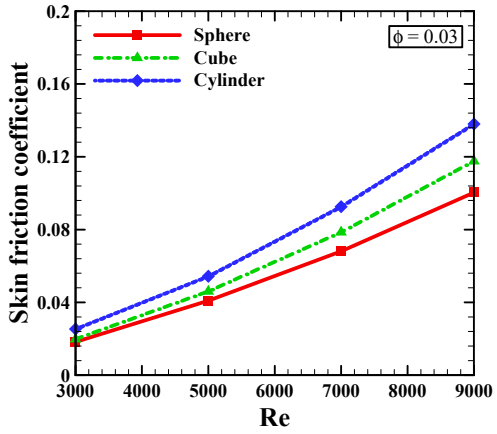

(**c**) Friction coefficient in ϕ=0.03

Figure 8. Friction coefficient vs. Re for a porosity coefficient of 0.7 and for different volume fractions in a microchannel with a square cross-section.

4.5. Average Nusselt Number in the Microchannel with the Triangular Cross-Section

The Nu versus Re for various NF concentrations is shown in Figure 9 for a spherical nanoparticle and triangular microchannel. As shown in this figure, the Nu increases with growing Re and decreases by increasing the NF concentration.

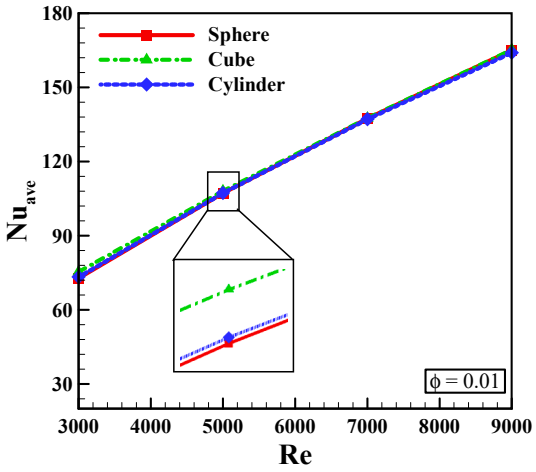

(**a**) Average Nusselt number in ϕ=0.01

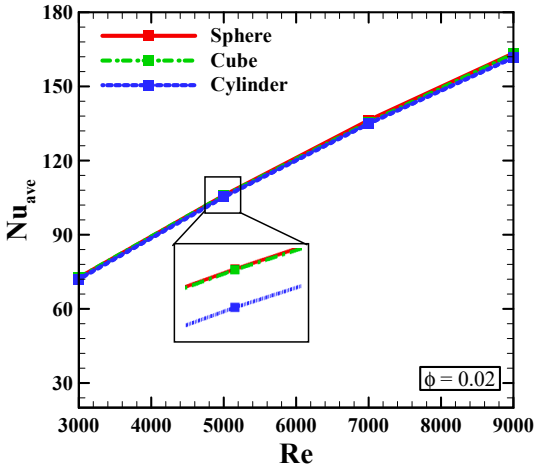

(**b**) Average Nusselt number in ϕ=0.02

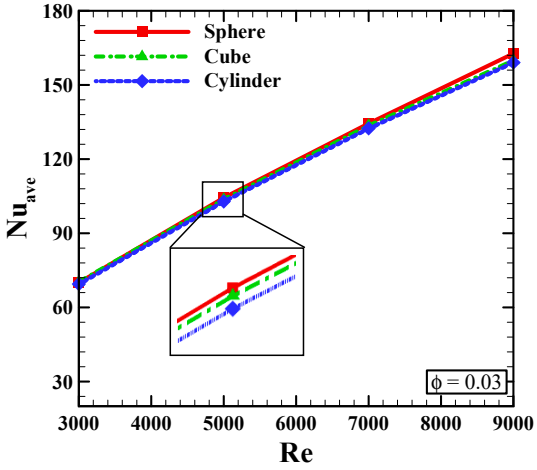

(**c**) Average Nusselt number in ϕ=0.03

Figure 9. Nu_{ave} vs. Re for a porosity coefficient of 0.7 and for different volume fractions in a microchannel with a triangular cross-section.

As shown in Figure 9, the Nu for cubic and cylindrical nanoparticles have trends identical to that of the spherical nanoparticle. In other words, the Nu is an increasing function of the Re and a decreasing function of the nanoparticle concentration.

4.6. Friction Coefficient for the Microchannel with the Triangular Cross-Section

The plots of friction coefficient and heat transfer shown in Figure 10 have identical behaviors for spherical, cylindrical, and cubic nanoparticles.

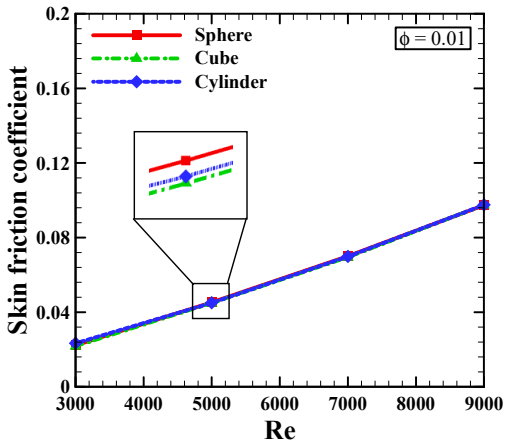

(**a**) Friction coefficient in ϕ=0.01

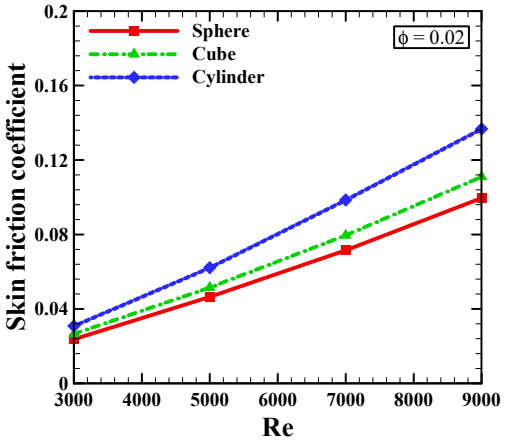

(**b**) Friction coefficient in ϕ=0.02

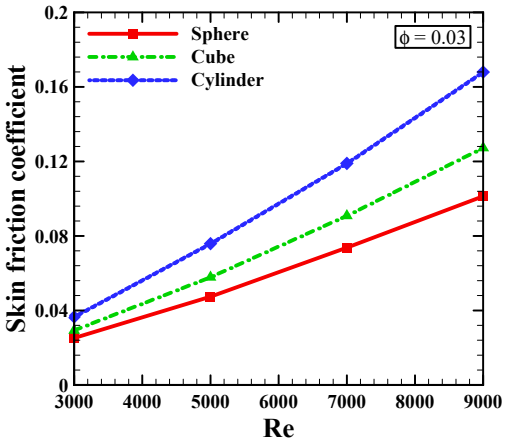

(**c**) Friction coefficient in ϕ=0.03

Figure 10. Friction coefficient vs. Re for a porosity coefficient of 0.7 and for different volume fractions in a microchannel with a triangular cross-section.

As can be seen from Figure 10, the friction coefficient is a growing function of Re and NF concentration for all cases, and the slope of the plot is steeper when cubic and cylindrical nanoparticles are used.

5. Conclusions

In this paper, the behavior of nanofluids in a microchannel filled with porous media is numerically investigated. The effects of nanoparticle shape, nanoparticle volume fraction, microchannel cross-section geometry, and Reynolds numbers on flow field and heat transfer were studied. The significant findings of this study are reported as below:

- The Nusselt number increases with growing Re for a porosity coefficient of 0.7, all three microchannel cross-sections, and all three nanoparticle shapes. Moreover, the Nusselt number decreases with growing NF concentration for the mentioned study cases.
- The Nusselt number for the cylindrical nanoparticle is smaller than those for the spherical and cubic nanoparticles for all volume fractions studied.
- For the cylindrical nanoparticle, the friction coefficient is reduced by Re enhancement. Furthermore, the friction coefficient is observed to be a growing function of nanoparticle volume fraction in the NF. This is exhibited more prominently at smaller Re values.
- In summary, this study shows that for a microchannel filled with porous media, the use of spherical nanoparticles results in a higher Nusselt number and a lower friction factor compared to other shapes of nanoparticles.
- In terms of the geometrical effect of the microchannel cross-section, the best heat transfer rate in the microchannel with triangular, rectangular, and circular cross-sections is recommended, respectively. Circular and triangular microchannels also have the lowest and highest friction coefficients, respectively.

This study showed that the use of microchannels filled with porous media with triangular cross-sections containing spherical nanoparticles can lead to the best heat transfer rate under the conditions studied.

Finally, it is suggested that the effects of different porosities and nanofluids with different nanoparticles be considered in future studies. Moreover, if this study is done experimentally, it can be very helpful in understanding the behavior of nanofluids in microchannels with porous media.

Author Contributions: The authors contributed the same to this MS. All authors have read and agreed to the published version of the manuscript.

Funding: This research received no external funding.

Conflicts of Interest: The authors declare no conflict of interest.

Abbreviations

Nomenclature

c_p	Specific heat capacity, J/K
Nu	Nusselt number
Re	Reynolds number
k	Thermal conductivity coefficient, W/m·K

Greek Symbols

ρ	Density, kg/m^3
ϕ	Nanoparticles volume fraction, Pa·s
μ	Dynamic viscosity
ε	Porosity coefficient

Subscripts

f	Base fluid
avg	Average
np	Nanoparticle
nf	Nanofluid

References

1. Hopp-Hirschler, M.; Shadloo, M.S.; Nieken, U. A Smoothed Particle Hydrodynamics Approach for Thermo-Capillary Flows. *Comput. Fluids* **2018**, *176*, 1–19. [CrossRef]
2. Dijvejin, Z.A.; Ghaffarkhah, A.; Sadeghnejad, S.; Sefti, M.V. Effect of silica nanoparticle size on the mechanical strength and wellbore plugging performance of SPAM/chromium (III) acetate nanocomposite gels. *Polym. J.* **2019**, *51*, 693–707. [CrossRef]
3. Afrand, M. Experimental study on thermal conductivity of ethylene glycol containing hybrid nano-additives and development of a new correlation. *Appl. Therm. Eng.* **2017**, *110*, 1111–1119. [CrossRef]
4. Hopp-Hirschler, M.; Shadloo, M.S.; Nieken, U. Viscous Fingering Phenomena in the Early Stage of Polymer Membrane Formation. *J. Fluid Mech.* **2019**, *864*, 97–140. [CrossRef]
5. Komeilibirjandi, A.H.; Raffiee, A.; Maleki, M.A.; Nazari, M.S. Thermal conductivity prediction of NFs containing CuO nanoparticles by using correlation and artificial neural network. *J. Therm. Anal. Calorim.* **2019**. [CrossRef]
6. Ghaffarkhah, A.; Afrand, M.; Talebkeikhah, M.; Sehat, A.A.; Moraveji, M.K.; Talebkeikhah, F.; Arjmand, M. On evaluation of thermophysical properties of transformer oil-based NFs: A comprehensive modeling and experimental study. *J. Mol. Liq.* **2020**, *300*, 112249. [CrossRef]
7. Shahrestani, M.I.; Maleki, A.; Shadloo, M.S.; Tlili, I. Numerical Investigation of Forced Convective Heat Transfer and Performance Evaluation Criterion of Al2O3/Water NF Flow inside an Axisymmetric Microchannel. *Symmetry* **2020**, *12*, 120. [CrossRef]
8. Karimi, A.; Afrand, M. Numerical study on thermal performance of an air-cooled heat exchanger: Effects of hybrid NF, pipe arrangement and cross section. *Energy Convers. Manag.* **2018**, *164*, 615–628. [CrossRef]
9. Parsa, S.M.; Rahbar, A.; Koleini, M.; Aberoumand, S.; Afrand, M.; Amidpour, M. A renewable energy-driven thermoelectric-utilized solar still with external condenser loaded by silver/NF for simultaneously water disinfection and desalination. *Desalination* **2020**, *480*, 114354. [CrossRef]
10. Sadeghi, R.; Shadloo, M.S.; Hopp-Hirschler, M.; Hadjadj, A.; Nieken, U. Three-dimensional lattice Boltzmann simulations of high density ratio two-phase flows in porous media. *Comput. Math. Appl.* **2018**, *75*, 2445–2465. [CrossRef]
11. Karimipour, A.; Afrand, M. Magnetic field effects on the slip velocity and temperature jump of nanofluid forced convection in a microchannel. *Proc. Inst. Mech. Eng. Part C J. Mech. Eng. Sci.* **2015**, *230*, 1921–1936. [CrossRef]
12. Nojoomizadeh, M.; Karimipour, A.; Firouzi, M.; Afrand, M. Investigation of permeability and porosity effects on the slip velocity and convection heat transfer rate of Fe3O4/water nanofluid flow in a microchannel while its lower half filled by a porous medium. *Int. J. Heat Mass Transf.* **2018**, *119*, 891–906. [CrossRef]
13. Liu, X.; Toghraie, D.; Hekmatifar, M.; Akbari, O.A.; Karimipour, A.; Afrand, M. Numerical investigation of nanofluid laminar forced convection heat transfer between two horizontal concentric cylinders in the presence of porous medium. *J. Therm. Anal. Calorim.* **2020**, *36*, 1–14. [CrossRef]
14. Arasteh, H.; Mashayekhi, R.; Ghaneifar, M.; Toghraie, D.; Afrand, M. Heat transfer enhancement in a counter-flow sinusoidal parallel-plate heat exchanger partially filled with porous media using metal foam in the channels' divergent sections. *J. Therm. Anal. Calorim.* **2019**, *34*, 1–17. [CrossRef]
15. Barnoon, P.; Toghraie, D.; Dehkordi, R.B.; Afrand, M. Two phase natural convection and thermal radiation of Non-Newtonian nanofluid in a porous cavity considering inclined cavity and size of inside cylinders. *Int. Commun. Heat Mass Transf.* **2019**, *108*, 104285. [CrossRef]
16. Jiang, P.; Fan, M.; Si, G.; Ren, Z. Thermal ± hydraulic performance of small scale micro-channel and porous-media heat-exchangers. *Int. J. Heat Mass Transf.* **2001**, *44*, 1039–1051. [CrossRef]
17. Hatami, M.; Ganji, D.D. Thermal and flow analysis of microchannel heat sink (MCHS) cooled by Cu—Water NF using porous media approach and least square method. *Energy Convers. Manag.* **2014**, *78*, 347–358. [CrossRef]
18. Ghazvini, M.; Shokouhmand, H. Investigation of a NF-cooled microchannel heat sink using Fin and porous media approaches. *Energy Convers. Manag.* **2009**, *50*, 2373–2380. [CrossRef]
19. Goodarzi, M. Investigation of permeability effect on slip velocity and temperature jump boundary conditions for FMWNT/Water NF flow and heat transfer inside a microchannel filled by a porous media. *Phys. E Low Dimens. Syst. Nanostruct.* **2017**, *97*, 226–238.

20. Ting, T.W.; Hung, Y.M.; Guo, N. International Journal of Heat and Mass Transfer Entropy generation of viscous dissipative NF flow in thermal non-equilibrium porous media embedded in microchannels. *Int. J. Heat Mass Transf.* **2015**, *81*, 862–877. [CrossRef]
21. Arabpour, A.; Karimipour, A.; Toghraie, D. Investigation into the effects of slip boundary condition on NF flow in a double-layer microchannel. *J. Anal. Calorim.* **2018**, *131*, 2975–2991. [CrossRef]
22. Hosseini, S.R.; Sheikholeslami, M. Investigation of the NF convective flow and entropy generation within a microchannel heat sink involving magnetic field. *Powder Technol.* **2019**, *351*, 195–202. [CrossRef]
23. Akbari, O.A.; Toghraie, D.; Karimipour, A.; Safaei, M.R.; Goodarzi, M.; Alipour, H.; Dahari, M. Investigation of rib's height effect on heat transfer and flow parameters of laminar water–Al2O3 nanofluid in a rib-microchannel. *Appl. Math. Comput.* **2016**, *290*, 135–153.
24. Karimipour, A.; Alipour, H.; Akbari, O.A.; Semiromi, D.T. Studying the Effect of Indentation on Flow Parameters and Slow Heat Transfer of Water-Silver Nano-Fluid with Varying Volume Fraction in a Rectangular Two-Dimensional Micro Channel. *Indian J. Sci. Technol.* **2015**, *8*, 51707. [CrossRef]
25. Reza, M.; Ali, O.; Marzban, A.; Toghraie, D. Growing heat transfer of non-Newtonian nano fluid in rectangular microchannel with triangular ribs. *Phys. E Low Dimens. Syst. Nanostruct.* **2017**, *93*, 167–178.
26. Arabpour, A.; Karimipour, A.; Toghraie, D. The study of heat transfer and laminar flow of kerosene/multi-walled carbon nanotubes (MWCNTs) NF in the microchannel heat sink with slip boundary condition. *J. Anal. Calorim.* **2018**, *131*, 1553–1566. [CrossRef]
27. Avramenko, A.A.; Tyrinov, A.I.; Shevchuk, I.V.; Dmitrenko, N.P.; Kravchuk, A.V.; Shevchuk, V.I. International Journal of Thermal Sciences Mixed convection in a vertical circular microchannel. *Int. J. Sci.* **2017**, *121*, 1–12.
28. Gao, C.; Jian, Y. Analytical solution of magnetohydrodynamic flow of Jeffrey fluid through a circular microchannel. *J. Mol. Liq.* **2015**, *211*, 803–811. [CrossRef]
29. El Mghari, H. Experimental and numerical investigations of local condensation heat transfer in a single square microchannel under variable heat flux. *Int. Commun. Heat Mass Transf.* **2016**, *71*, 197–207. [CrossRef]
30. Kiyasatfar, M.; Pourmahmoud, N. International Journal of Thermal Sciences Laminar MHD flow and heat transfer of power-law fl uids in square microchannels. *Int. J. Therm. Sci.* **2016**, *99*, 26–35. [CrossRef]
31. Ferrari, A.; Magnini, M.; Thome, J.R. International Journal of Heat and Mass Transfer Numerical analysis of slug flow boiling in square microchannels. *Int. J. Heat Mass Transf.* **2018**, *123*, 928–944. [CrossRef]
32. Behnampour, A.; Akbari, O.A.; Safaei, R.; Ghavami, M.; Marzban, A. Analysis of heat transfer and nanofluid fluid flow in microchannels with trapezoidal, rectangular and triangular shaped ribs. *Phys. E Low Dimens. Syst. Nanostruct.* **2017**, *19*, 25–36.
33. Wang, Y.; Shin, J.; Woodcock, C.; Yu, X.; Peles, Y. International Journal of Heat and Mass Transfer Experimental and numerical study about local heat transfer in a microchannel with a pin fin. *Int. J. Heat Mass Transf.* **2018**, *121*, 534–546. [CrossRef]
34. Dejam, M. Derivation of dispersion coefficient in an electro-osmotic flow of a viscoelastic fluid through a porous-walled microchannel. *Chem. Eng. Sci.* **2019**, *204*, 298–309. [CrossRef]
35. Dejam, M. Hydrodynamic dispersion due to a variety of flow velocity profiles in a porous-walled microfluidic channel. *Int. J. Heat Mass Transf.* **2019**, *136*, 87–98. [CrossRef]
36. Olayiwola, S.O.; Dejam, M. Experimental study on the viscosity behavior of silica nanofluids with different ions of electrolytes. *Ind. Eng. Chem. Res.* **2020**, *59*, 3575–3583. [CrossRef]
37. Olayiwola, S.O.; Dejam, M. Interfacial energy for solutions of nanoparticles, surfactants, and electrolytes. *Am. Inst. Chem. Eng. J.* **2020**, *66*, e16891. [CrossRef]
38. Maithani, R.; Kumar, A.; Zadeh, P.G.; Safaei, M.R.; Gholamalizadeh, E. Empirical correlations development for heat transfer and friction factor of a solar rectangular air passage with spherical-shaped turbulence promoters. *J. Therm. Anal. Calorim.* **2020**, *139*, 1195–1212. [CrossRef]
39. Nunes, J.M.; Souza, R.R.; Rodrigues, A.R.; Reza Safaei, M.; Cardoso, E.M. Influence of coated surfaces and gap size on boiling heat transfer of deionized water. *J. Braz. Soc. Mech. Sci. Eng.* **2020**, *42*, 1–14. [CrossRef]
40. Faraz, N.; Khan, Y.; Lu, D.C.; Goodarzi, M. Integral Transform Method to Solve the Problem of Porous Slider without Velocity Slip. *Symmetry* **2019**, *11*, 791. [CrossRef]
41. Safaei, M.R.; Goshayeshi, H.R.; Chaer, I. Solar Still Efficiency Enhancement by Using Graphene Oxide/Paraffin Nano-PCM. *Energies* **2019**, *12*, 2002. [CrossRef]
42. Maleki, H.; Safaei, M.R.; Alrashed, A.A.A.A.; Kasaeian, A. Flow and heat transfer in non-Newtonian nanofluids over porous surfaces. *J. Therm. Anal. Calorim.* **2019**, *135*, 1655–1666. [CrossRef]

43. Maleki, H.; Alsarraf, J.; Moghanizadeh, A.; Hajabdollahi, H.; Safaei, M.R. Heat transfer and nanofluid flow over a porous plate with radiation and slip boundary conditions. *J. Cent. South Univ.* **2019**, *26*, 1099–1115. [CrossRef]
44. Goshayeshi, H.R.; Safaei, M.R. Effect of absorber plate surface shape and glass cover inclination angle on the performance of a passive solar still. *Int. J. Numer. Methods Heat Fluid Flow* **2019**. [CrossRef]
45. Hamid, M.; Mohammad, R.S.; Abdullah, A.; Alibakhsh, K. Flow and heat transfer in non-Newtonian NFs over porous surfaces. *J. Therm. Anal. Calorim.* **2019**, *135*, 1655–1666.
46. Ahmadi, M.H.; Mohseni-Gharyehsafa, B.; Ghazvini, M.; Goodarzi, M.; Jilte, R.D.; Kumar, R. Comparing various machine learning approaches in modeling the dynamic viscosity of CuO/water nanofluid. *J. Therm. Anal. Calorim.* **2020**, *139*, 2585–2599. [CrossRef]
47. Akbari, O.A.; Mohammad, R.S.; Marjan, G.; Noreen, S.K.; Majid, Z.; Gholamreza, A.S.S.; Mahidzal, D. A modified two-phase mixture model of nanofluid flow and heat transfer in a 3-D curved microtube. *Adv. Powder Technol.* **2016**, *27*, 2175–2185. [CrossRef]
48. Hosseini, S.M.; Safaei, M.R.; Estellé, P.; Jafarnia, S.H. Heat transfer of water-based carbon nanotube NFs in the shell and tube cooling heat exchangers of the gasoline product of the residue fluid catalytic cracking unit. *J. Therm. Anal. Calorim.* **2020**, *140*, 351–362. [CrossRef]
49. Maleki, H.; Safaei, M.R.; Togun, H.; Dahari, M. Heat transfer and fluid flow of pseudo-plastic NF over a moving permeable plate with viscous dissipation and heat absorption/generation. *J. Therm. Anal. Calorim.* **2019**, *135*, 1643–1654. [CrossRef]
50. Bahiraei, M.; Salmi, H.K.; Safaei, M.R. Effect of employing a new biological NF containing functionalized graphene nanoplatelets on thermal and hydraulic characteristics of a spiral heat exchanger. *Energy Convers. Manag.* **2019**, *180*, 72–82. [CrossRef]
51. Hamlehdar, M.; Kasaeian, A.; Safaei, M.R. Energy Harvesting from Fluid Flow using Piezoelectrics: A Critical Review. *Renew. Energy* **2019**, *143*, 1826–1838. [CrossRef]
52. Bahiraei, M.; Mazaheri, N.; Aliee, F.; Safaei, M.R. Thermo-hydraulic performance of a biological NF containing graphene nanoplatelets within a tube enhanced with rotating twisted tape. *Powder Technol.* **2019**, *355*, 278–288. [CrossRef]
53. Mahian, O.; Kianifar, A.; Zeinali, S.; Wongwises, S. International Journal of Heat and Mass Transfer First and second laws analysis of a minichannel-based solar collector using boehmite alumina NFs: Effects of nanoparticle shape and tube materials. *Heat Mass Transf.* **2014**, *78*, 1166–1176. [CrossRef]
54. Abdollahzadeh, M.; Sedighi, A.A.; Esmailpour, M. Stagnation Point Flow of NFs Towards Stretching Sheet Through a Porous Medium with Heat Generation. *J. Nanofluids* **2018**, *7*, 1–7. [CrossRef]
55. Arjun, K.S.; Rakesh, K. Heat Transfer Enhancement Using Alumina NF in Circular Micro Channel. *J. Eng. Sci. Technol.* **2017**, *12*, 265–279.